www.nature.com/cdd

CDDpress

ARTICLE

Check for updates

PRMT4 promotes ferroptosis to aggravate doxorubicin-induced cardiomyopathy via inhibition of the Nrf2/GPX4 pathway

Yilong Wang[1,8], Shu Yan[2,3,8], Xuemei Liu[4], Fei Deng[5], Pengchao Wang[6], Liuye Yang[6], Lizhi Hu[6], Kai Huang[6,7]✉ and Jiangui He[1]✉

Doxorubicin (DOX), a commonly used antitumor agent, is often accompanied by its dosage-dependent cardiotoxicity, which incorporates ferroptosis in its pathogenesis. Protein arginine methyltransferase 4 (PRMT4) is a transcription regulator involved in the modulation of oxidative stress and autophagy, but its role in DOX-induced cardiomyopathy (DIC) and ferroptosis remains elusive. Herein, we aimed to investigate the involvement and the underlying mechanisms of PRMT4 in the pathogenesis of DIC. Our present study revealed that the expression level of PRMT4 was markedly decreased in DOX-treated cardiomyocytes. Interestingly, it is noted that PRMT4 overexpression accelerated ferroptosis to aggravate DIC, while its gene disruption or pharmaceutical inhibition exhibited the opposite effect. Mechanistically, our observation demonstrated that PRMT4 interacted with the nuclear factor erythroid 2-related factor 2 (Nrf2) to promote its enzymatic methylation, which restricted the nuclear translocation of Nrf2 and subsequently suppressed the transcription of glutathione peroxidase 4 (GPX4). Importantly, the detrimental role of PRMT4 in DOX-induced cardiomyocyte ferroptosis was abolished by Nrf2 activation or Fer-1 administration. Collectively, our data reveal that PRMT4 inhibits Nrf2/GPX4 signaling to accelerate ferroptosis in DIC, suggesting that targeting PRMT4 may present as a potential preventive strategy against the development of DIC.

Cell Death & Differentiation (2022) 29:1982–1995; https://doi.org/10.1038/s41418-022-00990-5

INTRODUCTION

Doxorubicin (DOX) is a widely used chemotherapeutic drug for various types of neoplasms [1]. However, the clinic administration of DOX is largely restricted by its dosage-dependent cardiotoxicity, which is characterized by cardiomyocyte loss, progressive cardiac enlargement, and ultimately congestive heart failure [2]. Patients receiving long-term DOX therapies develop heart dysfunction even at a lower dosage. It was estimated that approximately 26% of patients progressed to heart failure when receiving DOX at a cumulative dose over 550 mg/m^2 [2]. Therefore, uncovering the underlying mechanism and exploring potential preventive strategies for this adverse effect is urgently needed. Previous publications indicated that the pathogenesis of DOX-induced cardiomyopathy (DIC) incorporated various factors, including oxidative stress, mitochondrial disruption, and autophagy [3]. Recently, it is noted that ferroptosis, a unique type of regulated cell death, is an essential process in the progression of DIC.

Ferroptosis, a new form of non-apoptotic cell death, is characterized by the iron-dependent activation of lipoxygenase and the consequential cell death induced by excessive lipid peroxidation [4]. It has been validated that ferroptosis is ignited in various types of pathological scenarios, including myocardial ischemia-reperfusion injury, neurodegenerative diseases, acute kidney injury, chemotherapy-induced cancer cell death, and DIC [5–9]. The pathogenesis of ferroptosis is complicated, and recent investigations demonstrated that multiple transcription factors are involved, including p53, NUPR1, and nuclear factor erythroid 2-related factor 2 (Nrf2) [10, 11]. Importantly, as a key anti-ferroptotic transcription regulator, Nrf2 restored redox homeostasis through the induction of multiple antioxidant response element (ARE)-containing genes, including glutathione peroxidase 4 (GPX4), a potent enzyme catalyzing lethal lipid peroxide into nontoxic lipid alcohol [12–14]. Interestingly, it was reported that Nrf2 was intimately related to the pathogenesis of DIC [14, 15]. In comparison with the intensive investigations of transcription factors in ferroptosis, the research related to transcription cofactors is quite limited.

Protein arginine methyltransferase 4 (PRMT4), also termed coactivator-associated arginine methyltransferase 1 (CARM1), is a multifunctional transcription cofactor relevant to cell differentiation, metabolism, apoptosis, and oxidative stress [16–19]. Wang et al. revealed that PRMT4 catalyzed the methylation of MDH1 in arginine residue to regulate NADPH production and redox balance [20]; Besides, Kim et al. found that PRMT4 knockdown attenuated oxidative stress-induced injury in retinal pigment epithelial cells

[1]Department of Cardiology, The First Affiliated Hospital of Sun Yat-sen University, Guangzhou, China. [2]Guangzhou Institute of Pediatrics, Guangzhou Women and Children's Medical Center, Guangzhou Medical University, Guangzhou, China. [3]Heart Center and Institute of Pediatrics, Guangzhou Women and Children's Medical Center, Guangzhou Medical University, Guangzhou, China. [4]Department of functional medicine, Hunan Provincial Maternal and Child Health Care Hospital, Changsha, China. [5]Department of Urology, Second Xiangya Hospital, Central South University, Changsha, China. [6]Clinic Center of Human Gene Research, Union Hospital, Tongji Medical College, Huazhong University of Science and Technology, Wuhan, China. [7]Department of Cardiology, Union Hospital, Tongji Medical College, Huazhong University of Science and Technology, Wuhan, China. [8]These authors contributed equally: Yilong Wang and Shu Yan. ✉email: unionhuangkai@163.com; hejiangui@163.com

Edited by P Salomoni

Received: 4 August 2021 Revised: 18 March 2022 Accepted: 18 March 2022
Published online: 5 April 2022

[19]. Additionally, it was corroborated by Huang et al. that PRMT4, in cooperation with PRMT1, modulated ferritin (a key regulator of iron metabolism) expression to enhance cellular antioxidant response in the presence of arsenic [21]. In regard to the essential roles of oxidative perturbation and iron metabolism disruption in ferroptosis as mentioned above, we speculated that PRMT4 might be involved in the progression of ferroptosis.

The role of PRMT4 in cardiac disorders was poorly investigated, our recent publication demonstrated that PRMT4 overexpression exacerbated cardiomyocytes apoptosis and worsen cardiac function following myocardial infarction [17], but its role in the model of DIC has not been reported. In the current study, we aim to investigate the pathobiology of PRMT4 in cardiomyocytes ferroptosis and DIC.

MATERIALS AND METHODS

Animals

All animal procedures were approved by the Institutional Animal Care and Use Committees of the Sun Yat-Sen University and complied with the Guide for the Care and Use of Laboratory Animals published by the US National Institutes of Health. For cardiomyocyte-specific PRMT4 overexpression and knockdown in vivo, a total of 200 μl adeno-associated virus 9 (AAV9) carrying PRMT4 under the cTnT promoter (AAV-PRMT4) or short hairpin RNA (shRNA) against PRMT4 (AAV-shPRMT4) was applied at a dose of 1×10^{11} viral genome particles per mouse via tail vein injection. AAV9 carrying negative control (AAV-NC) and scramble shRNA (AAV-shNC) were used as controls. Male C57BL/6 J mice aged 8 to 10 weeks were used in the present study. A total of 2 weeks after AAV9 injection, the DIC model was established through a single injection of DOX (15 mg/kg, MedChemExpress). For the rescue or inhibitor experiment, Ferrostatin-1 (Fer-1, a specific inhibitor of ferroptosis, 2 mg/kg, MedChemExpress), or TP-064 (a selective inhibitor of PRMT4, 10 mg/kg, MedChemExpress) was intraperitoneally injected 2 h before DOX insult. The sequence of the mouse shPRMT4 was as follows: m-shPRMT4-1, 5′-TCAGGGACATGTCTGCTTATT-3′, m-shPRMT4-2, 5′-GCCTGAGCAAGTGGACATTAT-3′.

Cell culture and treatment

Primary neonatal rat ventricular myocytes (NRVMs) were isolated from 1- to 2-day-old Sprague-Dawley rat hearts digested with type 2 collagenase (Worthington). Then, the lysates were centrifuged through a discontinuous Percoll gradient. The cells were cultured in Dulbecco's Modified Eagle Medium (DMEM) supplemented with 10% fetal bovine serum (FBS) and antibiotics at 37 °C in a humidified atmosphere with 5% CO2. For DOX or RSL3 treatment, cells were transfected with indicated adenovirus for 48 h and then treated with DOX (2 μM) or RSL3 (0.5 μM) for another 24 h. For rescue experiment in vitro, Fer-1 (2 μM) was added 1 h before DOX treatment. H9C2 cardiomyocyte-like cell line was obtained from ATCC.

Cell viability analysis

Cell viability was determined using the CellTiter-Glo luminescent Cell Viability Assay (Promega) according to the manufacturer's instructions. Briefly, after treatment, cells were incubated with the test compound and equilibrated at room temperature for 30 min. Then CellTiter-Glo reagent was added to induce cell lysis and luminescence was recorded.

Virus preparation

Lentivirus encoding negative control (NC), Fbxo9 (LV-Fbxo9), or adenovirus encoding NC (Ad-NC), PRMT4 (Ad-PRMT4), scramble shRNA (Ad-shNC), and PRMT4 shRNA (Ad-shPRMT4) was applied to infect NRVMs in vitro, while the recombinant AAV system (AAV-NC, AAV-PRMT4, AAV-shNC, and AAV-shPRMT4) was employed to transduce cardiomyocyte in vivo via tail vein injection. All virus was provided by Vigene Biosciences. The targeting sequence of shRNA against rat PRMT4 was as follows: r-PRMT4-1, 5′-GCAGGCAGTCCTTCATCAT- 3′, r-PRMT4-2, 5′-GCACCTACCAGCGTGCAAT- 3′.

Echocardiography

Before and after DOX injection (day 7), Mice were anesthetized with continuous inhaled isoflurane (1%), and the heart rates were maintained at 500–600 beats/min. Transthoracic echocardiography was performed by an experienced technologist blind to the study protocol using a VEVO-1100 machine (Visual Sonics) and an M-mode Doppler. Echocardiographic parameters including left ventricular ejection fraction (LVEF), fraction shortening (FS), and ventricular dimensions (LVEDD) were measured.

Histological analysis

Heart tissues were fixed in 4% paraformaldehyde solution and embedded in paraffin. Then the heart tissues were cut into sequential slices. Paraffin sections were subjected to Masson staining for the detection of fibrotic area. For immunofluorescence staining, cells were fixed in 4% paraformaldehyde and permeabilized with 0.5% Triton X-100. Then the coverslips were blocked and incubated with the indicated antibodies or reagents as follows: PRMT4 (Bethyl Laboratories), cTnT (Abcam), Tom20 (Proteintech), MitoTracker (Thermo Fisher). FerroOrange (DOJINDO) and Lyso-Tracker (Beyotime) were used for live cell staining. Images were obtained using the fluorescence microscope (Olympus) and analyzed by the Image-Pro Plus 6.0 software (Media Cybernetics).

RNA extraction and quantitative real-time PCR (qPCR)

Total RNA was isolated from tissue or cells using RNAiso Plus (Takara), and 1 ug RNA was reverse-transcribed to cDNA with a PrimeScript™ RT reagent kit (Takara). Then, qPCR was performed with ChamQTM Universal SYBR® qPCR Master Mix (Vazyme) on an ABI PRISM 7900 Sequence Detector System (Applied Biosystems). 18 S rRNA was used as an internal control. Primers used in this study were listed as follows: PRMT4, forward: 5′-ATGATGCAGGACTATGTGCG-3′, reverse: 5′-AAATTTTCCTGGCTCCTGCT-3′, 18 S, forward: 5′-TTGACGGAAGGGCACCACCAG-3′, reverse: 5′-GCACCACC ACCCA CGGAATCG-3′.

Western blot

Western blot was performed as described previously [17]. Briefly, hearts or cardiomyocytes were lysed using RIPA buffer containing a complete protease inhibitor cocktail (Roche). Protein concentrations were determined using a BCA protein assay kit (Thermo Scientific). Proteins were then electrophoresed in SDS–PAGE and transferred on a PVDF membrane. After incubation in 5% non-fat milk, membranes were immunoblotted with the following antibodies: PRMT4 (Cell Signaling Technology), nuclear receptor coactivator 4 (NCOA4, Bethyl Laboratories), GPX4 (Bimake), Nrf2 (Cell Signaling Technology), Histone H3 (Abclonal), Immunoglobulin G (IgG, Cell Signaling Technology) Asymmetric Di-Methyl Arginine Motif (ADMA, Cell Signaling Technology), β-tubulin (Abcam), GAPDH (Abcam). A Clinx imaging system (Shanghai) was used to detect the chemiluminescence signal.

Nuclear-cytoplasmic fractionation

After treatment, harvest cells (10 cm dish) by scraping in PBS followed by centrifugation (500 g, 5 min). Add 500 μl hypotonic buffer (10 mM Tris pH 7.4, 10 mM KCl, 1.5 mM $MgCl_2$, 1 mM EDTA) to resuspend cells and leave on ice for 20 min with occasional mixing. Pass the cell suspension through a 25 G needle 25 times using a 1 ml syringe. Centrifuge at 500 g for 10 min. Transfer the supernatant (SN-1) to a new tube. Disperse the pellet with 500 μl of hypotonic buffer and pass through a 25 G needle for 50 times. Centrifuge and keep the pellet as nucleus fraction. Centrifuge SN-1 at 3000 g for 10 min and transfer the supernatant to a new tube (SN-2). Centrifuge SN-2 at 100,000 g for 30 min and transfer to a new tube. Finally, centrifuge the supernatant at 100,000 g for 30 min again and keep the final supernatant as cytosol fraction. The nucleus and cytosol fraction were then used for immunoblotting.

Biochemical detection

Serum was collected and the concentrations of creatine kinase isoenzymes (CK-MB), lactate dehydrogenase (LDH), and aspartate aminotransferase (AST) were measured with indicated kits (Nanjing Jiancheng) according to the manufacturer's instructions.

Malondialdehyde (MDA) and GSH level measurement

Freshly isolated heart tissue (30 mg) was used for MDA measurement with a kit (Beyotime) according to the manufacturer's instructions. To assess GSH level in vitro and in vivo, cardiomyocyte or heart lysate (30 mg) was used to detect the level of GSH through a kit (Beyotime) as described previously [22].

In vitro methylation assay

GST fusion protein GST-Nrf2 (Abcam) and purified recombinant Flag-PRMT4 (Active Motif) were used for in vitro methyltransferase assay as described previously [6]. Briefly, we incubated 1 μg of GST-Nrf2 with 1 μg of Flag-PRMT4 and 10 μM S-adenosyl-L-methionine (SAM, sigma) in 30 ul of methylation buffer (25 mM NaCl, 25 mM Tris-HCl, pH 8.8) for 2 h at 30 °C. Proteins were boiled with SDS loading buffer and subjected to immunoblotting analysis.

Iron assay

The content of iron (Fe^{2+} or total Fe) was measured according to the manufacturer's instructions (Abcam). Briefly, cells or tissue were homogenized in 5–10 volumes of Iron Assay Buffer and centrifuged, the supernatant was collected in a fresh microfuge tube. For the iron (Fe^{2+}) assay, add 5 μl of Assay Buffer to each sample. Add 5 μl of Iron Reducer to each sample for total iron assay. Mix and incubate at 37 °C for 30 min. Then add 100 μl Iron Probe to each well and incubate at 37 °C for 60 min. Measure output immediately on a colorimetric microplate reader (OD 593 nm).

GST pulldown

Equal amounts of GST or GST-Nrf2 were incubated with Flag-tagged PRMT4 for 4 h at 4 °C in GST binding buffer (50 mM Tris, pH 8.0, 0.1% NP40, 0.5 mM DTT, 10% Glycerol supplemented with protease inhibitors). Next, 30 ul pre-washed glutathione agarose (Santa Cruz) were added with rotation at 4 °C for 2 h. After six washes with GST binding buffer, the mixture was boiled and subjected to immunoblotting analysis.

Plasmid construction

The plasmid used in this study was bought from Addgene (USA). The enzyme-inactive form of PRMT4 ($PRMT4^{E266Q}$) was constructed using the Mut Express® II Fast Mutagenesis Kit (Vazyme) according to the manufacturer's instructions. Nrf2 truncated domains were amplified from full-length human Nrf2 cDNA and subcloned into the pcDNA3.1-3 × Flag construct.

Measurement of GPX4 activity

GPX4 activity was determined as previously described [23]. Cells or heart tissue (20 mg) were homogenized in 200 μl of lysis buffer. The lysates were then centrifuged at 15,000 g for 15 min at 4 °C, and the supernatants were collected. The protein concentration was determined. For GPX4 activity, 50 μl of supernatant was added into 1 ml of assay buffer (5 mM EDTA, 5 mM reduced glutathione, 0.1% Triton X-100, and 180 IU/ml glutathione reductase, and 160 mM NADPH/H^+, pH 7.8). After incubation for 5 min at 22 °C, 5 ul of 30 mM cumene hydroperoxide (Sangon) was added. The readings were recorded at an absorbance of 340 nm and measured every 10 s. GPX4 activity was then calculated.

TdT-mediated dUTP nick-end labeling (TUNEL) assay and cell morphology analysis

A TUNEL assay kit (Roche) was used to detect apoptosis index of the primary cardiomyocytes under DOX treatment (2 μM) and cardiac tissues after DOX (15 mg/kg) injection in accordance with the manufacturer's instructions. Images were captured by a fluorescence microscope (Olympus) and analyzed by the Image-Pro Plus 6.0 software (Media Cybernetics). For cell morphology studies, NRVMs were examined by phase-contrast light microscopy 24 h after DOX treatment.

Measurement of reactive oxygen species (ROS) production

The levels of intracellular ROS were determined using DCFH-DA staining in vitro and DHE staining in vivo, respectively. The cells or cryosections were washed with PBS and incubated with DCFH-DA or DHE for 30 min at 37 °C in the dark. Images were observed from five random fields per section by a fluorescence microscope (Olympus) and analyzed using the Image-Pro Plus 6.0 software (Media Cybernetics).

Co-immunoprecipitation (co-IP) assay

Co-IP was performed as described previously [24]. Briefly, tissue and cells were lysed with lysis buffer (150 mM NaCl, 50 mM Tris-HCl, pH 8.0, 5% glycerol, 1.0% NP40, 1 mM MgCl2, and complete protease inhibitors). The lysates were then incubated with indicated antibodies at 4 °C overnight and 30 μl of protein A/G beads (Beyotime) were added for another 2 h on a rotator. Immunoprecipitates were centrifuged and washed six times with wash buffer at 4 °C. The pellets were boiled and subjected to immunoblotting analysis.

Luciferase reporter assay

For luciferase assay, the GPX4 promoter (−1322-13) was amplified by PCR from the Rat genomic DNA and subcloned into the pGL3.0-basic vector (Promega) using an In-Fusion HD cloning kit (Takara). In total, 500 ng of each indicated plasmid was co-transfected with an internal control construct, pRL-TK (Renilla luciferase reporter plasmid, Promega), into H9C2 cardiomyocyte-like cells. A total of 24 h later, cell lysates were harvested and measured using the dual-luciferase assay system (Promega). Primers used to amplify Rat GPX4 promoter were as follows: forward: 5′-CCGCCAAGCCCTCCTACCA-3′, reverse: 5′-ATGCCCGCCCGTCTGTGC-3′.

Chromatin immunoprecipitation assay (ChIP)

The ChIP assay was conducted using a commercially available kit (Millipore) according to the manufacturer's instructions. In brief, cells were crosslinked with 1% formaldehyde for 10 min. After glycine (0.125 M) quenching, the cell pellets were lysed in lysis buffer and subjected to sonication for 5 min. The lysates were then centrifuged and incubated with indicated antibodies overnight at 4 °C. Immunocomplexes were captured with 30 μl of protein A/G sepharose on a rotator at 4 °C for 2 h. Beads were washed and eluted in the elution buffer. The supernatant was reverse-crosslinked at 65 °C overnight and then digested with proteinase K for 4 h at 55 °C. ChIP and input DNA were then purified and analyzed by qPCR. The value of enrichment was calculated relative to input and the ratio to IgG. The following primers were used in ChIP assays. r-GPX4 (ChIP), forward: 5′-CTAGCCTGGGCTACATGAGA-3′; reverse: 5′-GAGGGCTGCAGA-CAGTTATCC-3′.

Statistical analysis

SPSS 16.0 and Graphpad prism 8.0 was used for statistical analysis. All values were reported as mean ± standard deviation. The Student's t-test was used to compare two groups and multi-group comparisons were performed by one-way analysis of variance (ANOVA) with Bonferroni post hoc analysis. All experiments were conducted at least three times. $P < 0.05$ was considered statistically significant.

RESULTS

PRMT4 is downregulated in DIC

Post-translational modifications, such as phosphorylation and methylation, play key roles in maintaining cardiac homeostasis [25, 26]. However, studies related to methylation modification in DOX-induced cardiomyopathy are still lacking. We focused on arginine methylation-related PRMT members (PRMT1-9) and found that PRMT4 was most abundant in the murine heart (Supplementary Fig. S1a, b). In this regard, we decided to examine specifically the expression of PRMT4 in the model of DIC. In vitro, a time-dependent decrease of PRMT4 expression was observed in DOX-treated cardiomyocytes, as validated by immunoblot studies (Fig. 1a, b). Similarly, the expression of PRMT4 was also substantially downregulated in DOX-treated hearts (Fig. 1d, e). However, our qRT-PCR analysis revealed that the mRNA expression of PRMT4 remained unchanged, suggesting that other post-transcriptional mechanisms were incorporated in the downregulation of PRMT4 (Fig. 1c). Recently, one publication claimed that Fbxo9, an E3 ubiquitin ligase, was involved in the modulation of PRMT4 stability [27]. Within expectation, our data showed that DOX insult increased the level of Fbxo9 (Supplementary Fig. S2a). Further immunoblot assay revealed that Fbxo9 overexpression decreased the expression of PRMT4 in cardiomyocytes in a dose-dependent manner (Supplementary Fig. S2b, c), suggesting that Fbxo9 might be upstream of PRMT4 after DOX stress. To investigate the localization of PRMT4 in the heart, immunofluorescence analysis was performed, which revealed that PRMT4 co-localized with cTnT, a specific marker for cardiomyocyte (Supplementary Fig. S3a). The localization of PRMT4 was further confirmed by immunohistochemistry studies (Supplementary Fig. S3a–c), indicating that PRMT4 localized both in the cytoplasm

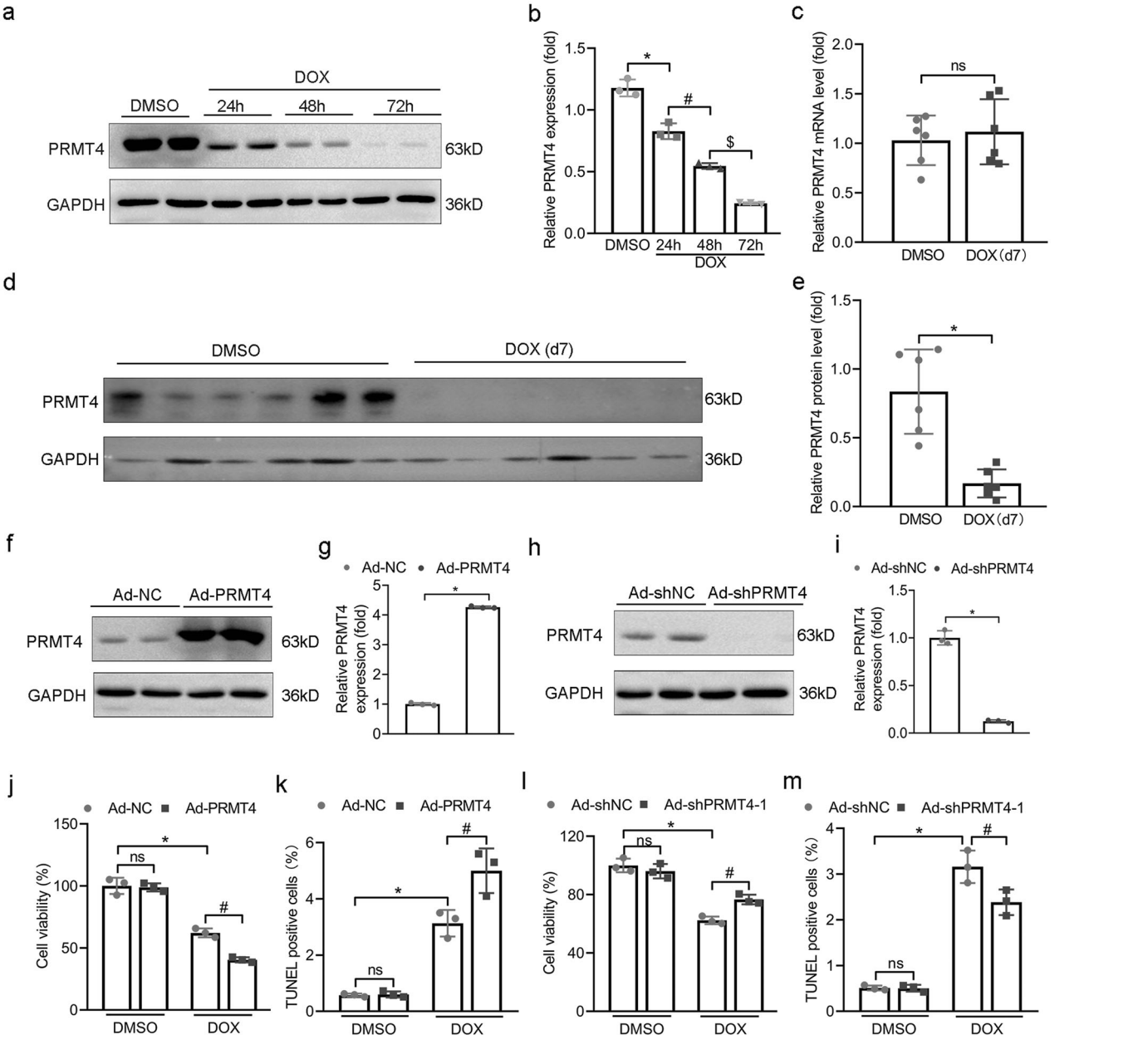

Fig. 1 PRMT4 is involved in DIC. NRVMs were treated with DOX (2 μM) for 24, 48, and 72 h. **a** Representative western blot of PRMT4 was shown; **b** Quantitative analysis of the protein level of PRMT4. $^{*}P < 0.05$, $^{\#}P < 0.01$, $^{\$}P < 0.001$; **c** The mRNA level of PRMT4 was determined; **d** Representative western blot of PRMT4 in the myocardium 7 days after DOX (15 mg/kg) injection; **e** Quantitative analysis of the protein level of PRMT4 in DOX-treated hearts. $^{*}P < 0.001$; NRVMs were infected with adenovirus (Ad-NC, Ad-PRMT4, Ad-shNC, or Ad-shPRMT4) and treated with DOX (2 μM) for 24 h, **f**–**i** Adenovirus-mediated PRMT4 overexpression or depletion in vitro was detected by western blot and quantitatively analyzed; Representative images were shown; **j**, **l** Cell viability was detected. $^{*}P < 0.001$, $^{\#}P < 0.01$ (**j**). $^{*}P < 0.001$, $^{\#}P < 0.001$ (**l**); **k**, **m** TUNEL positive cells were determined. $^{*}P < 0.001$, $^{\#}P < 0.05$ (**k**). $^{*}P < 0.001$, $^{\#}P < 0.05$ (**m**). ns, not significant.

and nucleus of the cardiomyocyte. Besides, our immunofluorescence and immunohistochemistry studies also verified the decline of PRMT4 in the myocardium following DOX treatment (Supplementary Fig. S3a, b). Altogether, the initial findings indicated that PRMT4 was conceivably downregulated during the progression of DIC.

PRMT4 promotes DOX-mediated cardiomyocyte damage in vitro

To evaluate the role of PRMT4 in DOX-induced cardiomyocyte injury, various types of methods were employed in in vitro studies. Adenovirus was used to manipulate the expression level of PRMT4 in cardiomyocytes (Fig. 1f–i). Our phase-contrast microscopic analysis demonstrated that DOX treatment led to conceivable cell death (as indicated by the number of live cells and shrunken cells), which was attenuated by PRMT4 knockdown but accentuated by PRMT4 overexpression (Supplementary Fig. S4a, b). Similarly, a marked decrease in cell survival rate was observed in DOX-treated cardiomyocytes, and PRMT4 overexpression exacerbated, while its gene disruption mitigated the cellular survival (Fig. 1j, l, and Supplementary Fig. S5a). Moreover, PRMT4 overexpression aggravated DOX-induced DNA damage in cardiomyocytes, as validated by TUNEL staining, while it was considerably alleviated by PRMT4

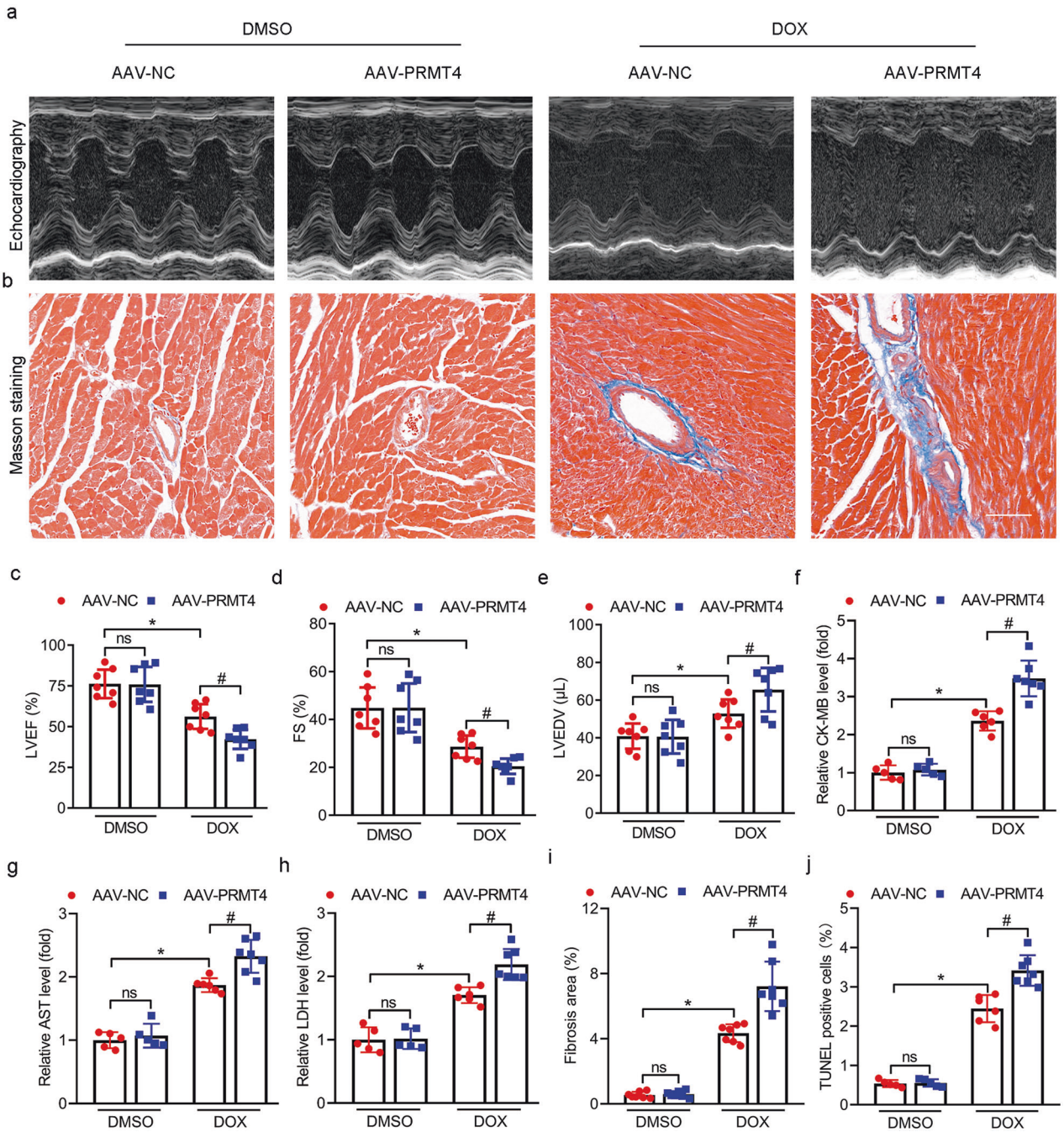

Fig. 2 PRMT4 overexpression aggravates DIC in vivo. AAV-NC or AAV-PRMT4 were applied via tail vein injection and the DIC model was established 14 days later. **a** Representative images of M-mode echocardiograms; **b** Representative Masson staining images. **c**–**e** Quantitative analysis of LVEF (**c**, $^{*}P < 0.01$, $^{\#}P < 0.01$), FS (**d**, $^{*}P < 0.01$, $^{\#}P < 0.01$), and LVEDV (**e**, $^{*}P < 0.05$, $^{\#}P < 0.05$) by echocardiography; **f**–**h** Quantitative analysis of serum CK-MB (**f**, $^{*}P < 0.001$, $^{\#}P < 0.001$), AST (**g**, $^{*}P < 0.001$, $^{\#}P < 0.01$), and LDH (**h**, $^{*}P < 0.001$, $^{\#}P < 0.01$); **i** Quantitative analysis of fibrosis area. $^{*}P < 0.001$, $^{\#}P < 0.01$; **j** Quantitative analysis of TUNEL positive cells by immunofluorescence staining. $^{*}P < 0.001$, $^{\#}P < 0.05$.

knockdown (Fig. 1k, m, and Supplementary Fig. S5b). Taken together, the results above implied that PRMT4 promoted DOX-mediated cardiomyocyte injury in vitro.

PRTM4 aggravates the progression of DIC in vivo

To determine the role of PRMT4 in vivo, AAV9 was applied via tail vein injection to manipulate the expression profile of PRMT4 [17]. The DIC model was established, cardiac function and the extent of myocardial injury were analyzed. As shown in Fig. 2, DOX treatment led to a conceivable decline of left ventricular ejection fraction (LVEF) and fractional shortening (FS), as well as elevation of left ventricular end-diastolic volume (LVEDV) compared to the control (AAV-NC), as indicated by echocardiography assessment. Interestingly, these aberrant alterations were accelerated by cardiac-specific PRMT4 overexpression and alleviated by PRMT4 gene disruption (Fig. 2a, c–e, 3a, c–e, and Supplementary Fig. S6a, c–e). Various types of injury-related biomarkers, including CK-MB, LDH, and AST, were detected to further evaluate cardiac injuries. As shown in our serum biochemistry assay, PRMT4 overexpression substantially promoted DOX-induced increase of CK-MB, LDH, and AST, while its knockdown attenuated their changes (Fig. 2f–h, 3f–h, and Supplementary Fig. S6f–h). In addition, the fibrotic state of

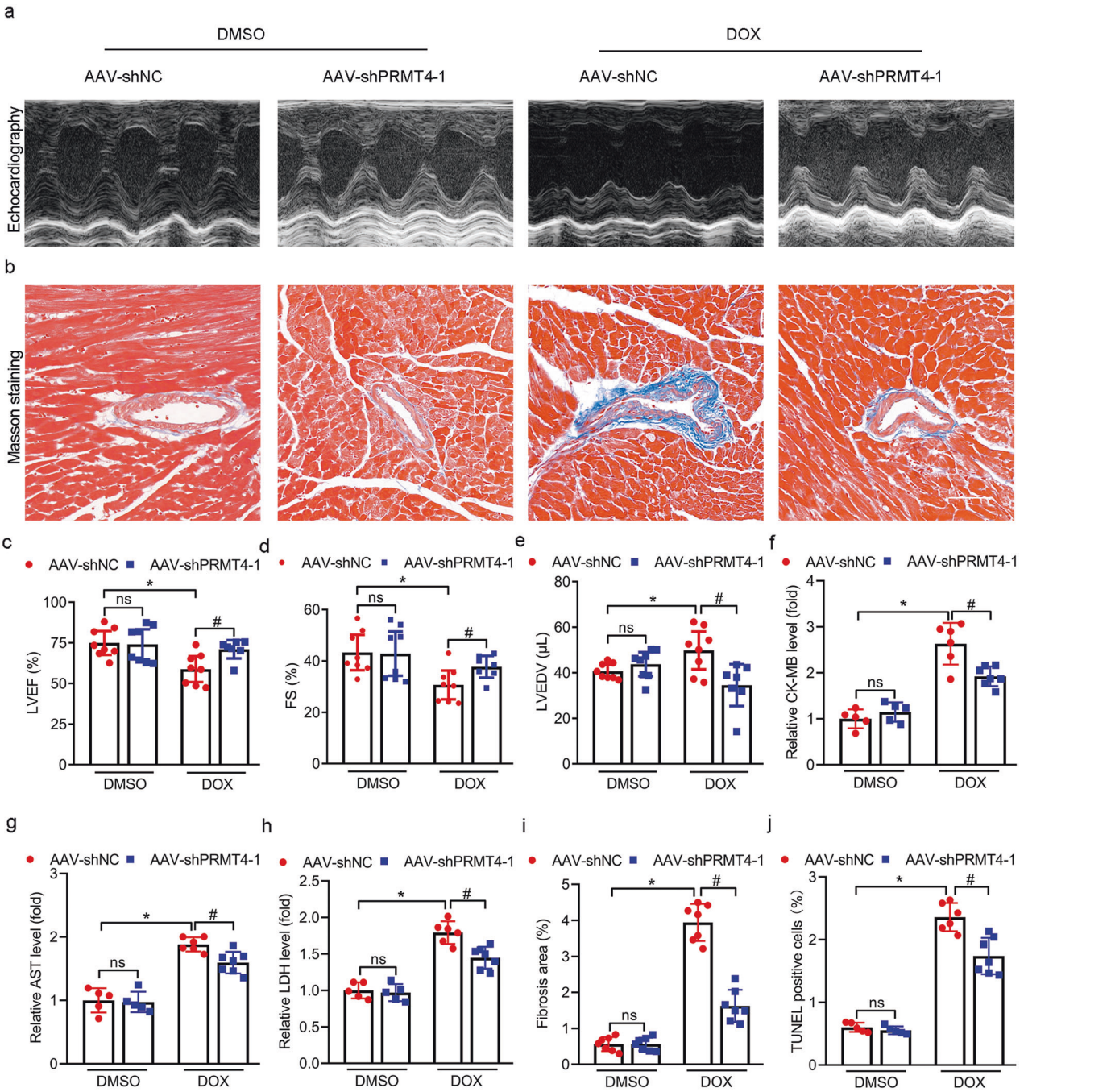

Fig. 3 PRMT4 disruption alleviates DIC in vivo. AAV-shNC or AAV-shPRMT4 were applied via tail vein injection and the DIC model was established 14 days later **a** Representative images of M-mode echocardiograms; **b** Representative Masson staining images. **c**–**e** Quantitative analysis of LVEF (**c**, $^{*}P < 0.01$, $^{\#}P < 0.05$), FS (**d**, $^{*}P < 0.01$, $^{\#}P < 0.05$), and LVEDV (**e**, $^{*}P < 0.05$, $^{\#}P < 0.05$) by echocardiography; **f**–**h** Quantitative analysis of serum CK-MB (**f**, $^{*}P < 0.001$, $^{\#}P < 0.01$), AST (**g**, $^{*}P < 0.001$, $^{\#}P < 0.01$), and LDH (**h**, $^{*}P < 0.001$, #$P < 0.01$); **i** Quantitative analysis of fibrosis area, $^{*}P < 0.001$, $^{\#}P < 0.001$; **j** Quantitative analysis of TUNEL positive cells by immunofluorescence staining, $^{*}P < 0.001$, $^{\#}P < 0.01$.

murine hearts was investigated by Masson staining. Our analysis revealed that DOX administration resulted in cardiac fibrosis, which was aggravated by PRMT4 overexpression but mitigated by PRMT4 knockdown (Fig. 2b, i, 3b, i, and Supplementary Fig. S6b, i). Finally, the DNA damage analysis, as evaluated by TUNEL staining, demonstrated that PRMT4 overexpression deepened DOX-induced DNA breakdown in the myocardium, while its gene disruption ameliorated these aberrant alterations (Fig. 2j, 3j, and Supplementary Fig. S6j). More importantly, pharmaceutical inhibition of PRMT4 (TP-064, a selective inhibitor of PRMT4) alleviated DOX-induced cardiomyopathy (Supplementary Fig. S7a–g). Of note, cardiomyocyte size and survival rate were not affected by the expression profile of PRMT4 in the DIC model (Supplementary Fig. S8a–d and S9a, b). Taken together, the in vivo data indicates that PRMT4 promotes DOX-induced cardiac injury and exacerbated the progression of DIC.

PRMT4 promotes DOX-induced cardiomyocyte ferroptosis

Previous publications indicated that ferroptosis, a unique type of cell death characterized by iron overload and lipid peroxidation, was a

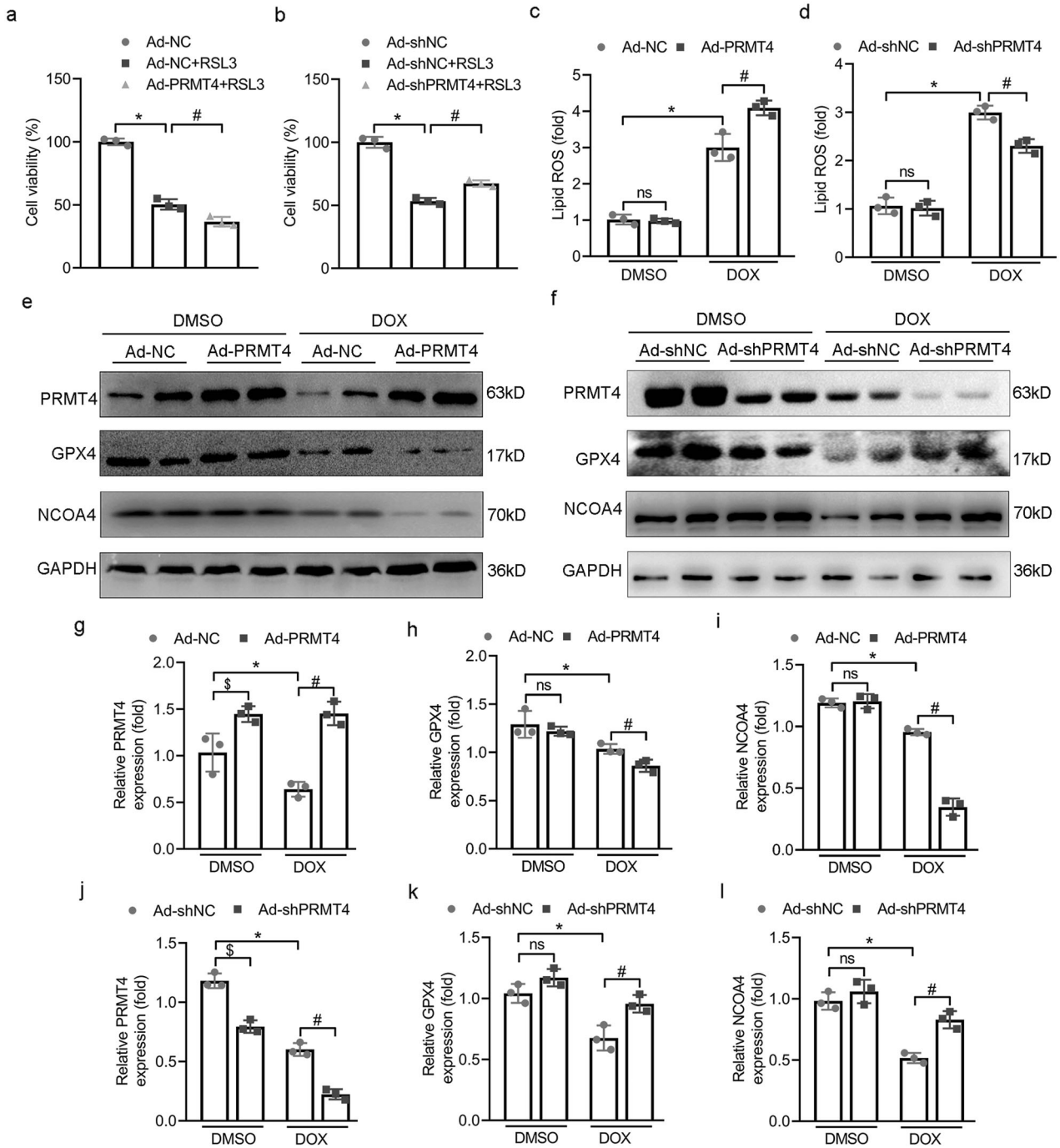

Fig. 4 PRMT4 promotes DOX-induced ferroptosis in vitro. NRVMs were infected with adenovirus (Ad-NC, Ad-PRMT4, Ad-shNC, or Ad-shPRMT4) and treated with RSL3 (0.5 μM) or DOX (2 μM) for 24 h. **a**, **b** Quantitative analysis of cell viability, $^{*}P < 0.001$, $^{\#}P < 0.05$ (**a**). $^{*}P < 0.001$, $^{\#}P < 0.01$ (**b**); **c**, **d** Cellular lipid ROS was determined, $^{*}P < 0.01$, $^{\#}P < 0.05$ (**c**). $^{*}P < 0.01$, $^{\#}P < 0.05$ (**d**); **e**, **f** Representative western blots of PRMT4, NCOA4, and GPX4 were shown; **g**, **j** Quantitative analysis of the protein level of PRMT4, $^{*}P < 0.05$, $^{\#}P < 0.001$, $^{\$}P < 0.05$ (**g**). $^{*}P < 0.001$, $^{\#}P < 0.001$, $^{\$}P < 0.01$ (**j**); **h**, **k** Quantitative analysis of the protein level of GPX4, $^{*}P < 0.05$, $^{\#}P < 0.05$ (**h**). $^{*}P < 0.01$, $^{\#}P < 0.05$ (**k**); **i**, **l** Quantitative analysis of the protein level of NCOA4, $^{*}P < 0.001$, $^{\#}P < 0.001$ (**i**). $^{*}P < 0.001$, $^{\#}P < 0.01$ (**l**).

vital process in the progression of DIC. Moreover, selective inhibition of ferroptosis significantly improved cardiac function after DOX administration [9, 28]. Herein, we first tried to investigate whether or not PRMT4 was incorporated in the modulation of ferroptosis in DOX-treated cardiomyocytes. Our initial analysis revealed that RSL3, a ferroptosis activator, led to a considerable decline in cardiomyocyte survival. Interestingly, this ferroptotic cell death was aggravated by PRMT4 overexpression and alleviated by PRMT4 disruption, suggesting that PRMT4 was involved in the process of ferroptosis (Fig. 4a, b). Next, DCFH-DA staining demonstrated that DOX treatment led to an overwhelming generation of ROS, a key marker of ferroptosis. Of note, the increased lipid ROS was accentuated by PRMT4 overexpression and attenuated by PRMT4 knockdown (Fig. 4c, d). In addition, other two markers related to ferroptosis, GPX4 (the end terminator of ferroptosis) and NCOA4 (the biomarker of ferritinophagy), were also investigated in our present studies [8, 29]. A simultaneous decline of GPX4 and NCOA4 was observed in cardiomyocytes following DOX treatment, and this change was aggravated by PRMT4 overexpression

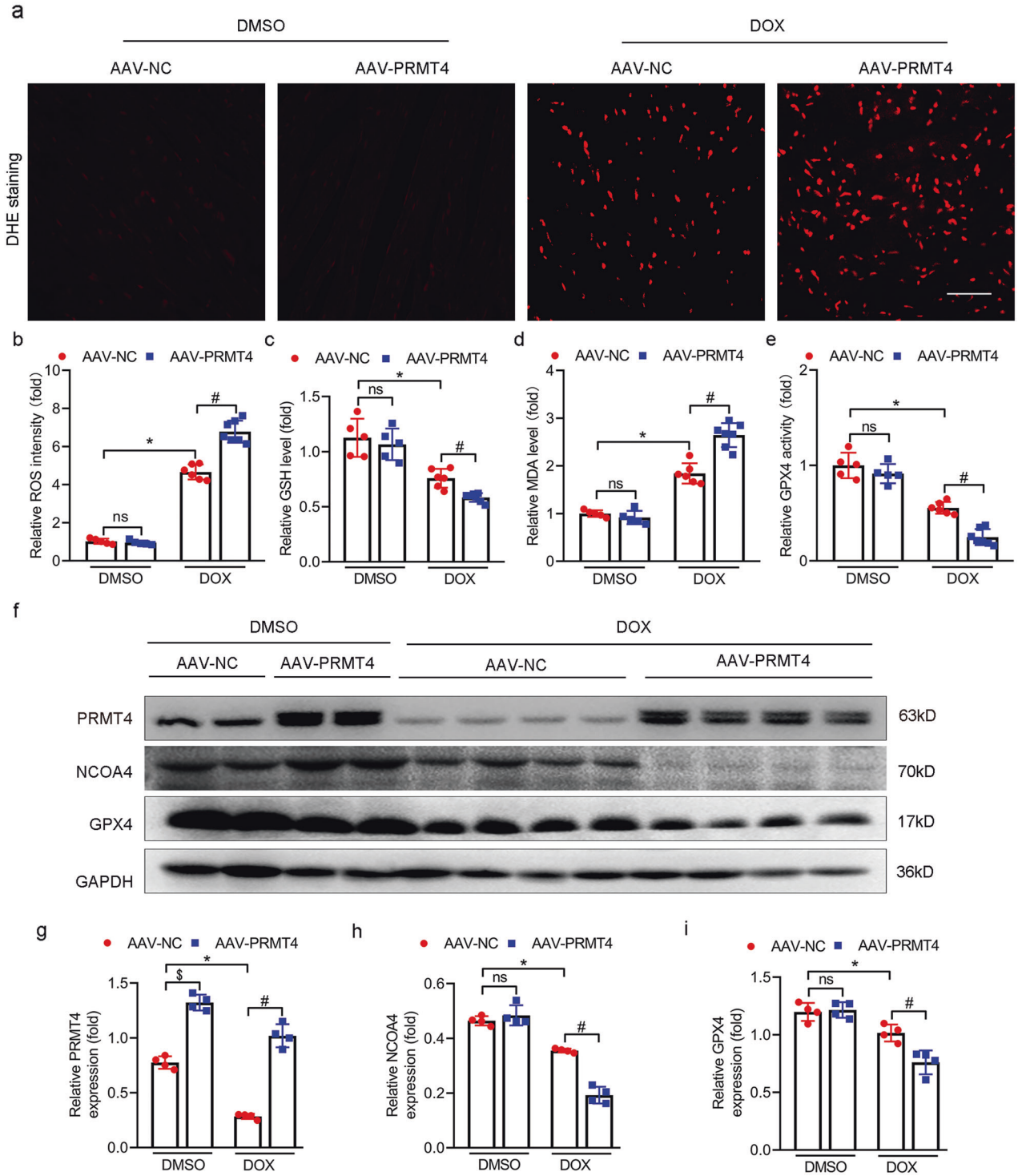

Fig. 5 PRMT4 overexpression promotes DOX-induced ferroptosis in vivo. AAV-PRMT4 or AAV-NC were applied via tail vein injection, 2 weeks later, DOX was injected intraperitoneally, then hearts were harvested for analysis on day 7. **a** Representative DHE staining images were shown; **b** Relative ROS intensity was statistically analyzed, $^{*}P < 0.001$, $^{\#}P < 0.001$; **c**–**e** Quantitative analysis of GSH level (**e**, $^{*}P < 0.01$, $^{\#}P < 0.001$), MDA level (**f**, $^{*}P < 0.001$, $^{\#}P < 0.001$), and GPX4 activity (**g**, $^{*}P < 0.001$, $^{\#}P < 0.001$); **f** Representative western blots of PRMT4, NCOA4, and GPX4 were shown; **g**–**i** Quantitative analysis of the protein level of PRMT4 (**g**, $^{*}P < 0.001$, $^{\#}P < 0.001$, $^{\$}P < 0.001$), NCOA4 (**h**, $^{*}P < 0.001$, $^{\#}P < 0.001$), and GPX4 (**i**, $^{*}P < 0.05$, $^{\#}P < 0.001$).

(Fig. 4e, g–i). Of note, the depletion of GPX4 and NCOA4 induced by DOX was conceivably attenuated by the loss of PRMT4 in cardiomyocytes (Fig 4f, j–l). Ferroptosis is characterized by mitochondrial shrunken and iron overload. Next, DOX-induced mitochondrial injury was detected by immunofluorescence analysis in vitro and in vivo. It was observed that DOX treatment led to significant mitochondrial damage, which was accentuated by PRMT4 overexpression but alleviated by PRMT4 knockdown (Supplementary Fig. S10a–d). In regard to the detection of intracellular iron, our results showed that DOX treatment increased the level of iron (Fe^{2+} and total

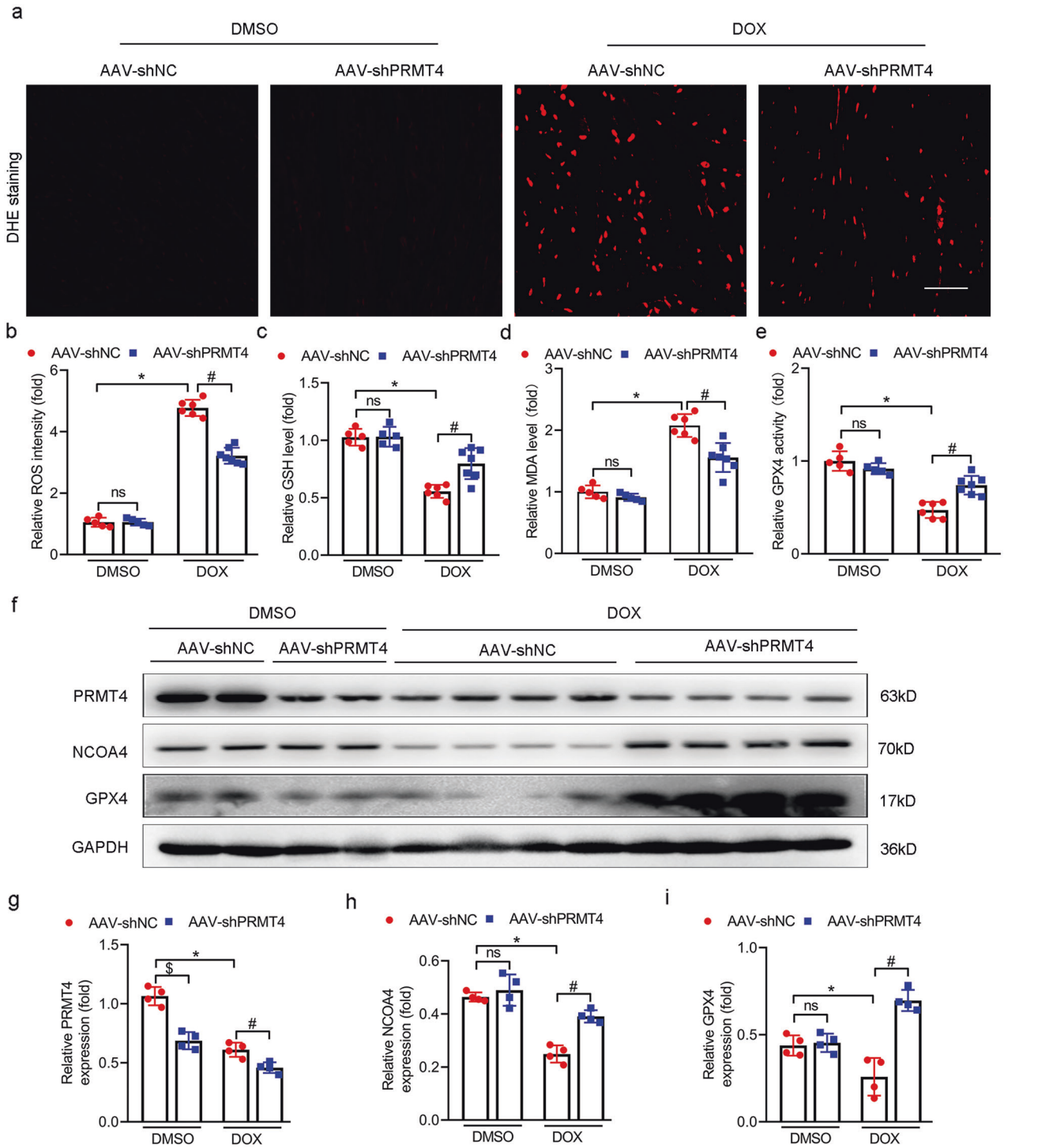

Fig. 6 PRMT4 disruption protects against DOX-induced ferroptosis in vivo. AAV-shPRMT4 or AAV-shNC were applied via tail vein injection, 2 weeks later, DOX was injected intraperitoneally, then hearts were harvested for analysis on day 7. **a** Representative DHE staining images were shown; **b** Relative ROS intensity was statistically analyzed, $^{*}P < 0.001$, $^{\#}P < 0.001$; **c-e** Quantitative analysis of GSH level (**c**, $^{*}P < 0.001$, $^{\#}P < 0.01$), MDA level (**d**, $^{*}P < 0.001$, $^{\#}P < 0.01$), and GPX4 activity (**e**, $^{*}P < 0.001$, $^{\#}P < 0.001$); **f** Representative western blots of PRMT4, NCOA4, and GPX4 were shown; **g-i** Quantitative analysis of the protein level of PRMT4 (**g**, $^{*}P < 0.001$, $^{\#}P < 0.01$, $^{\$}P < 0.001$), NCOA4 (**h**, $^{*}P < 0.001$, $^{\#}P < 0.001$), and GPX4 (**i**, $^{*}P < 0.05$, $^{\#}P < 0.01$).

iron), and this aberrant alteration was aggravated by PRMT4 introduction but attenuated by PRMT4 disruption. Besides, iron staining demonstrated that the elevated content of Fe^{2} was mainly localized in the lysosomes (Supplementary Fig. S11a–f). To further verify the dominant role of PRMT4 in DOX-induced cardiac ferroptosis, ferroptosis-related parameters were investigated in in vivo studies. Histological and biochemistry analysis revealed that DOX treatment resulted in increased production of ROS along with MDA and decreased level of GSH, indicating the generation of overwhelming lipid peroxidation. Interestingly, these changes were damped by

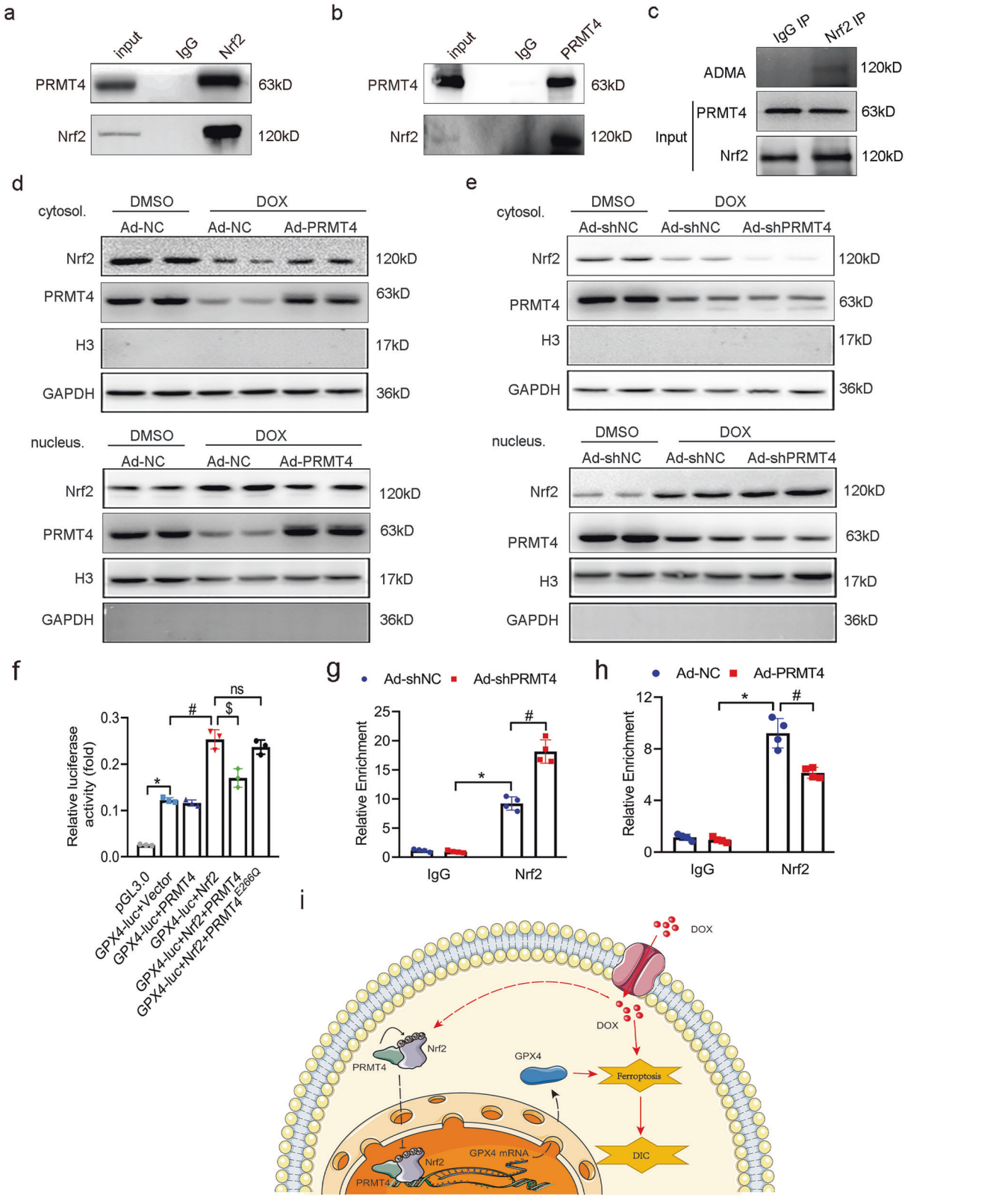

Fig. 7 PRMT4 transcriptionally controls GPX4 expression through Nrf2. a, **b** co-IP assay showed the interaction between PRMT4 and Nrf2 in NRVMs; **c** Cell lysates from NRVMs were incubated with anti-IgG or Nrf2 antibody, and followed by WB with anti-ADMA; **d**, **e** NRVMs were transfected with adenovirus, cells were harvested 24 h after DOX treatment and subjected to nuclear-cytoplasmic fractionation. Then, the protein level of Nrf2 in the nucleus and cytoplasm was determined respectively; **f** Luciferase assay was performed to analyze the effect of PRMT4 on Nrf2-mediated GPX4 promoter activation, $^{*}P < 0.001$, $^{\#}P < 0.001$, $^{\$}P < 0.05$; **g**, **h** H9C2 cells were transfected with adenovirus (Ad-NC, Ad-shNC, Ad-PRMT4, or Ad-shPRMT4) and ChIP assay was used to analyze the enrichment of Nrf2 on the rat GPX4 promoter loci with antibody against IgG or Nrf2. $^{*}P < 0.001$, $^{\#}P < 0.01$ (**g**), $^{*}P < 0.001$, $^{\#}P < 0.05$ (**h**); **i** Schematic model of the role and underlying mechanism of PRMT4 in the progression of DIC.

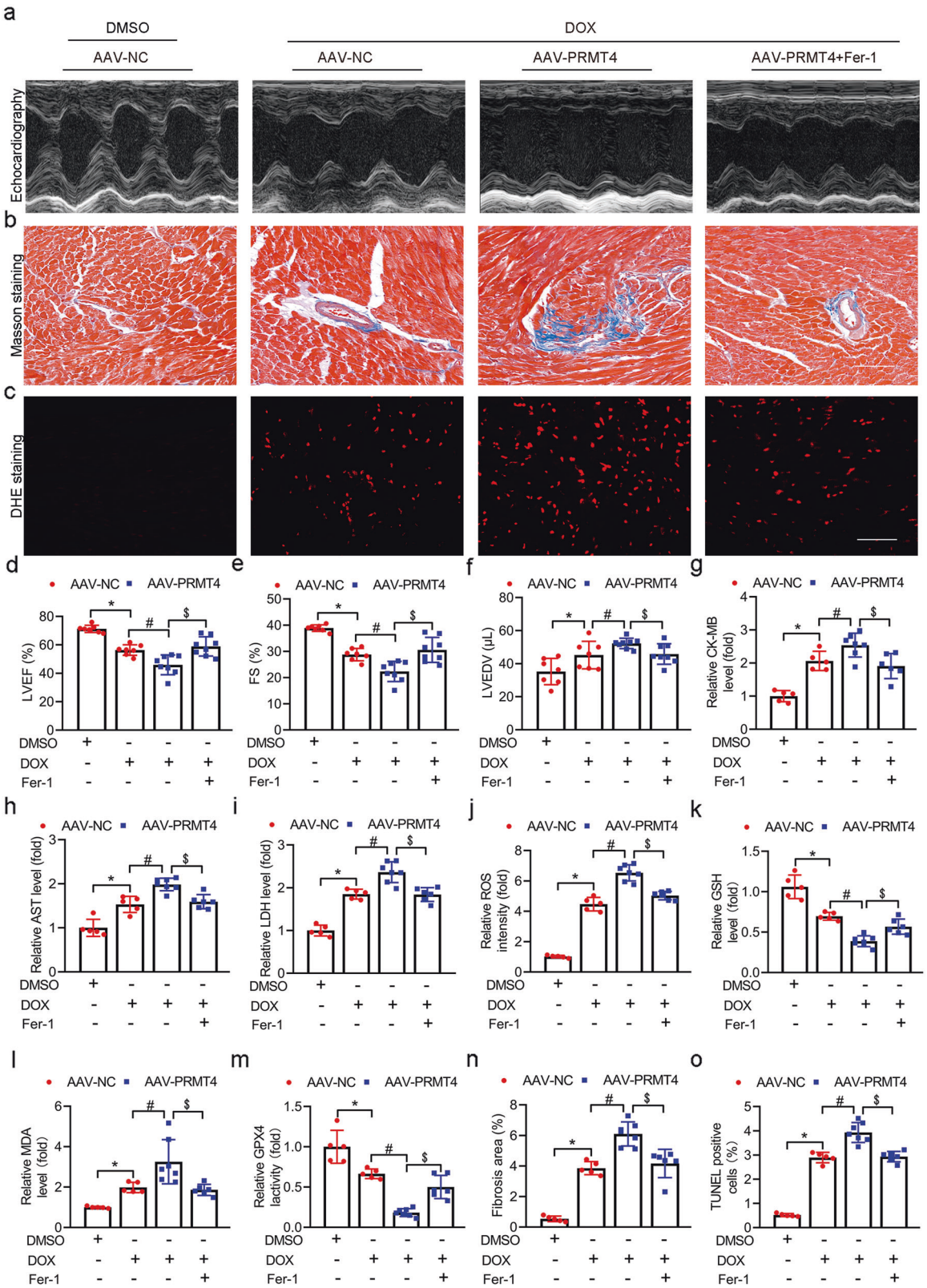

PRMT4 overexpression (Fig. 5a–d) but mitigated by its knockdown (Fig. 6a–d). In agreement with the findings in vitro, the decrease of NCOA4 and GPX4 was modulated by the expression profile of PRMT4 accordingly, as validated by immunoblotting studies (Fig. 5f–i and 6f–i). More importantly, GPX4 activity which was depressed upon the administration of DOX, was partially restored by PRMT4 knockdown but accentuated by its forced expression (Fig. 5e and 6e). Overall, these findings suggested that PRMT4 promoted ferroptosis to aggravate DOX-induced cardiomyocyte injury both in vitro and in vivo.

Fig. 8 Fer-1 administration abrogated the detrimental effect on DIC mediated by PRMT4. AAV-NC or AAV-PRMT4 were applied via tail vein injection, 2 weeks later, Fer-1 was injected intraperitoneally 2 h before establishment of the DIC model. **a** Representative images of M-mode echocardiograms; **b** Representative Masson staining images, Scale bar, 50 μm; **c** Representative DHE staining images were shown, Scale bar, 20 μm; **d**–**f** Quantitative analysis of LVEF (**d**, $^{*}P < 0.001$, $^{\#}P < 0.01$, $^{\$}P < 0.01$), FS (**e**, $^{*}P < 0.001$, $^{\#}P < 0.01$, $^{\$}P < 0.01$), and LVEDV (**f**, $^{*}P < 0.05$, $^{\#}P < 0.05$, $^{\$}P < 0.05$) by echocardiography; **g**–**i**; Quantitative analysis of serum CK-MB (**g**, $^{*}P < 0.001$, $^{\#}P < 0.05$, $^{\$}P < 0.05$), AST (**h**, $^{*}P < 0.01$, $^{\#}P < 0.001$, $^{\$}P < 0.001$), and LDH (**i**, $^{*}P < 0.001$, $^{\#}P < 0.01$, $^{\$}P < 0.001$); **j** Relative ROS intensity was statistically analyzed, $^{*}P < 0.001$, $^{\#}P < 0.001$, $^{\$}P < 0.001$; **k**–**m** Quantitative analysis of GSH level (**k**, $^{*}P < 0.001$, $^{\#}P < 0.01$, $^{\$}P < 0.01$), MDA level (**l**, $^{*}P < 0.001$, $^{\#}P < 0.05$, $^{\$}P < 0.05$), and GPX4 activity (**m**, $^{*}P < 0.001$, $^{\#}P < 0.001$, $^{\$}P < 0.001$); **n** Quantitative analysis of fibrosis area, $^{*}P < 0.001$, $^{\#}P < 0.001$, $^{\$}P < 0.01$; **o** Quantitative analysis of TUNEL positive cells by immunofluorescence staining, $^{*}P < 0.001$, $^{\#}P < 0.001$, $^{\$}P < 0.001$.

PRMT4 targets the Nrf2-GPX4 axis to aggravate DIC

Regarding the fact that PRMT4 acts as a key co-transcription factor, it is conceivable that PRMT4 participates in ferroptosis via the interaction with a certain transcription factor. Interestingly, it was reported that multiple transcription factors were involved in the modulation of ferroptosis [10, 11, 15], among which Nrf2 was the most investigated. Nrf2, a key anti-oxidant component, promotes the transcription of GPX4 to suppress ferroptosis [14]. As validated above, PRMT4 downregulated the expression of GPX4 in cardiomyocytes, we, therefore, assumed that PRMT4 might modulate the transcriptional activity of GPX4 through Nrf2. As anticipated, our co-IP and GST pulldown assay revealed that PRMT4 interacted with Nrf2 in cardiomyocytes (Fig. 7a, b and Supplementary Fig. S12a). Next, we mapped the specific domain of Nrf2 bound to PRMT4. A series of truncated forms of Nrf2 were generated, and the co-IP analysis identified that HA-tagged PRMT4 co-precipitated the second and third domain of Nrf2, indicating that the Neh4-6 region of Nrf2 mediated the interaction (Supplementary Fig. S12b). Since PRMT4 is a type I PRMT that asymmetrically dimethylates arginine residue of various proteins [24], we next explored whether Nrf2 was a novel substrate of PRMT4. NRVMs were subjected to co-IP with IgG or anti-Nrf2 antibodies, followed by immunoblotting with an antibody specific for ADMA. It was observed that methylated-Nrf2 was detected in the IP lysates, indicating the methylation of Nrf2 by PRMT4 in vivo (Fig. 7c). Further in vitro methylation assay demonstrated that Nrf2 was methylated by PRMT4, and this modification was significantly attenuated by TP-064. Noteworthily, Nrf2 could be methylated by PRMT1 as well, while PRMT5 was not involved (Supplementary Fig. S13a, b). Under basal conditions, Nrf2 localized in the cytoplasm and was degraded via the ubiquitin-proteasome pathway [30]. In agreement with the previous report, DOX treatment led to the translocation of Nrf2 from the cytoplasm to the nucleus. Interestingly, the nuclear accumulation of Nrf2 was significantly repressed by the introduction of PRMT4 and accelerated by its knockdown, as assessed by nuclear-cytoplasmic fractionation (Fig. 7d–e) and immunofluorescence analysis (Supplementary Fig. S14a, b). In addition, pre-treatment with TP-064 reversed the nuclear translocation disruption of Nrf2 by PRMT4 overexpression (Supplementary Fig. S15), indicating that the nuclear localization of Nrf2 was methylation-dependent. In addition, it was demonstrated by dual-luciferase and ChIP assay that PRMT4 overexpression suppressed Nrf2-mediated GPX4 expression (Fig. 7f–h). It is noteworthy that the enzyme-inactive PRMT4^{E266Q} failed to inhibit the transcription activity of Nrf2 (Fig. 7f), indicating the dominant role of PRMT4 on Nrf2 was intimately related to its enzymatic potency. Furthermore, pharmaceutical activation of Nrf2 by Bardoxolone (BARD) conceivably attenuated DOX-induced cardiomyocyte ferroptosis in the state of PRMT4 overexpression compared with control (Supplementary Fig. S16a–c). In this regard, we deemed that PRMT4 interacted with Nrf2 to catalyze its methylation and restrict its nuclear localization, which subsequently inhibited the expression of GPX4 to promote ferroptosis.

Fer-1 administration abrogated the detrimental effect on DIC mediated by PRMT4

Finally, to determine whether PRMT4-mediated cardiac injury was ferroptosis-dependent, Fer-1, a selective inhibitor of ferroptosis, was employed before DOX injection. Compared to control (AAV-NC), cardiac-specific overexpression of PRMT4 exhibited a significantly higher level of lipid peroxides in the hearts (Fig. 8c, j–m), severe myocardial damage (Fig. 8g–i) coupled with poor cardiac performance (Fig. 8a, b, d–f, n, o), while these detrimental changes were considerably alleviated after Fer-1 pre-treatment. Similarly, Fer-1 supplementation in vitro diminished PRMT4 overexpression-induced ROS production and cardiomyocyte death in the context of DOX stimulation (Supplementary Fig. S17a–c).

DISCUSSION

In the present study, we revealed a previously uncovered role of PRMT4 in DIC. We found that the expression level of PRMT4 was markedly decreased in DOX-treated cardiomyocytes and hearts. Besides, cardiac-restricted overexpression of PRMT4 aggravated, while its gene disruption or pharmaceutical inhibition mitigated, the progression of DIC by modulating the process of ferroptosis. Furthermore, selective inhibition of ferroptosis blocked the detrimental effect on DIC mediated by PRMT4. Mechanistically, we demonstrated that PRMT4 catalyzed the enzymatic methylation of Nrf2, leading to the restricted nuclear translocation of Nrf2 and decreased expression of the downstream ferroptosis-related gene GPX4. These findings thus highlighted a pivotal role of the cardiac PRMT4/Nrf2/GPX4 axis in the progression of DIC.

DOX, a widely used chemotherapeutic drug, elicits dosage-dependent cardiac toxicity, which often jeopardizes the quality of life and even causes life-threatening disorders [2]. Although the exact mechanism through which DOX exerts its toxic effects on cardiomyocytes remains elusive, various aspects of mechanisms have been proposed. The most accepted notion was that excessive DOX, accumulated in the mitochondria, interfered with multiple mitochondrial processes, leading to excessive ROS generation and oxidative stress-induced cell death subsequently [2, 31, 32]. Noteworthily, recent publications revealed that PRMT4 was involved in the modulation of redox perturbation [19, 20]. PRMT4 is a multifunctional transcription cofactor relevant to various bioprocesses, and our previous investigation showed that PRMT4 overexpression promoted hypoxia-induced cardiomyocyte apoptosis and worsen cardiac function following myocardial infarction [17]. In this regard, we speculated that PRMT4 might participate in the regulation of DOX-induced cardiomyocyte damage. In line with the previous evidence, our in vitro investigation showed that overexpression of PRMT4 was associated with a higher level of ROS along with a lower cardiomyocyte survival rate in the presence of DOX. Similarly, AAV-mediated cardiac PRTM4 overexpression in mice exhibited more ROS production, enhanced cardiac injury, and worse cardiac performance following DOX insult. Taken together, these data indicated that PRMT4 accelerated DOX-induced ROS production to exacerbate cardiac disruption.

Due to the intimate relationship between PRMT4 and ROS generation in the state of DIC, it is conceivable that PRMT4 might be involved in the modulation of ferroptosis. Ferroptosis was a newly identified form of non-apoptotic cell death characterized by iron-dependent overwhelming lipid peroxidation [4]. It has been validated that ferroptosis is implicated in various pathological

conditions, including chemotherapy-induced cancer cell death, acute kidney injury, and neurodegenerative diseases [4, 6, 7]. In 2019, Fang et al. initially reported that ferroptosis, rather than other forms of cell death, contributed to the occurrence of DIC [9]. Interestingly, this observation was further validated by another group of investigators, who presented that GPX4-transgenic mice exhibited improved cardiac performance following DOX administration by inhibiting ferroptosis [33]. However, the exact molecular network involved in DOX-induced ferroptosis remains elusive. Herein, our data presented that DOX treatment led to conceivable changes in ferroptosis-related markers, including NCOA4, GPX4, GSH, and MDA levels. Interestingly, those aberrant parameters were accentuated by PRMT4 overexpression but attenuated by its gene disruption. Taken together, we deemed that PRMT4 exacerbated DOX-induced cardiac injury by promoting ferroptosis.

Our recent publication showed that PRMT4 overexpression exacerbated cardiomyocytes apoptosis in the model of myocardial infarction [17]. To elucidate the distinct role of PRMT4 in DOX-induced apoptosis and ferroptosis, apoptosis-associated biomarkers in the cardiomyocytes were also investigated. It is manifested that PRMT4 overexpression promoted, while its gene disruption inhibited, DOX-induced cardiomyocyte apoptosis (Supplementary Fig. S18a–d), which was consistent with our previous published data [17]. These findings indicated that PRMT4 played a vital role both in DOX-induced apoptosis and ferroptosis. Similarly, a recent publication by Tadokoro et al. [33] found that both apoptosis and ferroptosis were involved in the DIC model. Their convincing work with in vitro investigation showed that the combined usage of zVAD (apoptosis inhibitor) and Fer-1 (ferroptosis inhibitor) almost completely abolished DOX-induced cardiomyocytes death, which highlighted the cooperative role of apoptosis and ferroptosis in the pathogenesis of DIC. In addition, their further investigation revealed that ferroptosis was independent of apoptosis in DOX-induced cardiomyocyte death. Apoptosis mainly peaked in the early phase (10 h), while ferroptosis proceeded to execute beyond 30 h following DOX treatment. Noteworthily, a recent study by Fang showed that Fer-1, but not apoptosis inhibitor (emricasan) affects the survival rate in the DIC model [9]. A possible explanation for this is that ferroptosis accounts for a higher ratio than apoptosis in the DIC model or caspase inhibition re-directs cells towards other mechanisms of cell death [34]. However, to what extent PRMT4 is involved in cardiomyocyte apoptosis and ferroptosis in the pathogenesis of DIC remains elusive, which needs further in-depth investigation.

Next, we proceed to try to figure out how PRMT4 participated in the occurrence of ferroptosis. PRMT4 is a multifunctional transcription co-activator [35] and it is conceivable that PRMT4 might regulate ferroptosis via the interaction with certain transcription factors. Recently, various transcription factors have been implicated in the pathogenesis of ferroptosis [36]. Jiang et al. reported that p53 suppressed the transcription of SLC7A11, resulting in escalated sensitivity to ferroptosis in cancer cell lines [10]. Besides, it was found by Liu et al. that NUPR1, a stress-inducible transcription factor, promoted ferroptosis resistance by transactivating the target gene lipocalin 2 (an ion transporter) [11]. Nrf2, an antioxidant transcription factor, maintains redox homeostasis via the induction of multiple downstream antioxidant target genes, including GPX4 and TXNRD1 [14]. Importantly, Nrf2 has been reported to be a key negative regulator of ferroptosis in hepatocellular carcinoma cells through activating multiple genes involved in lipid peroxides production and iron metabolism [37]. Moreover, another study showed that Nrf2 activation protected against ferroptosis in Friedreich's Ataxia by enhancing mitochondrial function and restoring redox balance [38]. As previously presented, PRMT4 modulated the expression of GPX4 in the presence of DOX, indicating that PRMT4 might interact with Nrf2. Indeed, our co-IP assay confirmed the interaction between PRMT4 and Nrf2 in cardiomyocytes. The finding was in accordance with the discovery that both PRMT4 and Nrf2 were present in the p300/CBP transcription complex [35, 39]. In addition, our further mechanistic study verified that Nrf2 could be methylated by PRMT4. However, this observation was inconsistent with the report by Liu, which presented that Nrf2 was not methylated by PRMT4 in HepG2 cells [40], possibly due to differences among the cell lines. Within expectation, our further mechanistic experiments validated that PRMT4 methylated Nrf2 to dominate the nuclear translocation of Nrf2 and the transcriptional activity of GPX4 in the presence of DOX. Actually, the protective role of Nrf2 in DIC has been extensively investigated [15]. Nordgren et al. demonstrated that DOX treatment led to Nrf2 activation and the expression of Nrf2-dependent antioxidant genes [41]. Also, it was reported by Li et al. that Nrf2 deletion in the heart exacerbated DOX-induced cardiomyopathy through promoting oxidative stress and autophagy [15]. Normally, the protective effect due to mild activation of Nrf2 after DOX challenge in the heart was not sufficient to overcome DOX-induced oxidative damage [42]. However, our finding that loss of PRMT4 in cardiomyocytes facilitated Nrf2's nuclear translocation and alleviated DOX-mediated cardiac injury indicated a threshold for Nrf2 activation in combating against the cardiotoxicity of DOX. Besides, this notion was further validated by the fact that Nrf2 agonist reverted the phenotype caused by PRMT4 overexpression. In aggregate, our findings disclosed the cardiac PRMT4/Nrf2/GPX4 axis in the progression of DIC.

In summary, we herein revealed a novel role of the PRMT4/Nrf2/GPX4 axis in the modulation of ferroptosis during the progression of DIC. This finding is of paramount significance in deciphering the molecular mechanism involved in DOX-induced ferroptosis, thus offering a potential target in preventing the development of DIC in clinical practice.

DATA AVAILABILITY

The data and material that support the findings of this study are available from the corresponding author upon reasonable request.

REFERENCES

1. Mohammadi M, Arabi L, Alibolandi M. Doxorubicin-loaded composite nanogels for cancer treatment. J Control Release. 2020;328:171–91.
2. Wallace KB, Sardao VA, Oliveira PJ. Mitochondrial determinants of doxorubicin-induced cardiomyopathy. Circ Res. 2020;126:926–41.
3. Kalyanaraman B. Teaching the basics of the mechanism of doxorubicin-induced cardiotoxicity: Have we been barking up the wrong tree? Redox Biol. 2020;29:101394.
4. Dixon SJ, Lemberg KM, Lamprecht MR, Skouta R, Zaitsev EM, Gleason CE, et al. Ferroptosis: an iron-dependent form of nonapoptotic cell death. Cell. 2012;149:1060–72.
5. Li W, Feng G, Gauthier JM, Lokshina I, Higashikubo R, Evans S, et al. Ferroptotic cell death and TLR4/Trif signaling initiate neutrophil recruitment after heart transplantation. J Clin Invest. 2019;129:2293–304.
6. Xu S, Zheng H, Ma R, Wu D, Pan Y, Yin C, et al. Vacancies on 2D transition metal dichalcogenides elicit ferroptotic cell death. Nat Commun. 2020;11:3484.
7. Deng F, Sharma I, Dai Y, Yang M, Kanwar YS. Myo-inositol oxygenase expression profile modulates pathogenic ferroptosis in the renal proximal tubule. J Clin Invest. 2019;129:5033–49.
8. Yang WS, SriRamaratnam R, Welsch ME, Shimada K, Skouta R, Viswanathan VS, et al. Regulation of ferroptotic cancer cell death by GPX4. Cell. 2014;156:317–31.
9. Fang X, Wang H, Han D, Xie E, Yang X, Wei J, et al. Ferroptosis as a novel target for protection against cardiomyopathy. Proc Natl Acad Sci. 2019;116:2672–80.
10. Jiang L, Kon N, Li T, Wang SJ, Su T, Hibshoosh H, et al. Ferroptosis as a p53-mediated activity during tumour suppression. Nature. 2015;520:57–62.
11. Liu J, Song X, Kuang F, Zhang Q, Xie Y, Kang R, et al. NUPR1 is a critical repressor of ferroptosis. Nat Commun. 2021;12:647.
12. Salazar M, Rojo AI, Velasco D, de Sagarra RM, Cuadrado A. Glycogen synthase kinase-3beta inhibits the xenobiotic and antioxidant cell response by direct phosphorylation and nuclear exclusion of the transcription factor Nrf2. J Biol Chem. 2006;281:14841–51.
13. Kinowaki Y, Kurata M, Ishibashi S, Ikeda M, Tatsuzawa A, Yamamoto M, et al. Glutathione peroxidase 4 overexpression inhibits ROS-induced cell death in diffuse large B-cell lymphoma. Lab Invest. 2018;98:609–19.
14. Dodson M, Castro-Portuguez R, Zhang DD. NRF2 plays a critical role in mitigating lipid peroxidation and ferroptosis. Redox Biol. 2019;23:101107.

15. Li S, Wang W, Niu T, Wang H, Li B, Shao L, et al. Nrf2 deficiency exaggerates doxorubicin-induced cardiotoxicity and cardiac dysfunction. Oxid Med Cell Longev. 2014;2014:1–15.
16. Chang NC, Sincennes MC, Chevalier FP, Brun CE, Lacaria M, Segales J, et al. The dystrophin glycoprotein complex regulates the epigenetic activation of muscle stem cell commitment. Cell Stem Cell. 2018;22:755–768.
17. Wang Y, Ju C, Hu J, Huang K, Yang L. PRMT4 overexpression aggravates cardiac remodeling following myocardial infarction by promoting cardiomyocyte apoptosis. Biochem Biophys Res Commun. 2019;520:645–50.
18. Zhong XY, Yuan XM, Xu YY, Yin M, Yan WW, Zou SW, et al. CARM1 methylates GAPDH to regulate glucose metabolism and is suppressed in liver cancer. Cell Rep. 2018;24:3207–23.
19. Kim DI, Park MJ, Choi JH, Kim IS, Han HJ, Yoon KC, et al. PRMT1 and PRMT4 regulate oxidative stress-induced retinal pigment epithelial cell damage in SIRT1-dependent and SIRT1-independent manners. Oxid Med Cell Longev. 2015;2015:617919.
20. Wang YP, Zhou W, Wang J, Huang X, Zuo Y, Wang TS, et al. Arginine methylation of MDH1 by CARM1 inhibits glutamine metabolism and suppresses pancreatic cancer. Mol Cell. 2016;64:673–87.
21. Huang BW, Ray PD, Iwasaki K, Tsuji Y. Transcriptional regulation of the human ferritin gene by coordinated regulation of Nrf2 and protein arginine methyltransferases PRMT1 and PRMT4. FASEB J. 2013;27:3763–74.
22. Wang Y, Lei T, Yuan J, Wu Y, Shen X, Gao J, et al. GCN2 deficiency ameliorates doxorubicin-induced cardiotoxicity by decreasing cardiomyocyte apoptosis and myocardial oxidative stress. Redox Biol. 2018;17:25–34.
23. Ingold I, Berndt C, Schmitt S, Doll S, Poschmann G, Buday K, et al. Selenium utilization by GPX4 is required to prevent hydroperoxide-induced ferroptosis. Cell. 2018;172:409–422.
24. Yan S, Hu J, Li J, Wang P, Wang Y, Wang Z. PRMT4 drives post-ischemic angiogenesis via YB1/VEGF signaling. J Mol Med. 2021;99:993–1008.
25. Smith LE, White MY. The role of post-translational modifications in acute and chronic cardiovascular disease. Proteom Clin Appl. 2014;8:506–21.
26. Pyun JH, Kim HJ, Jeong MH, Ahn BY, Vuong TA, Lee DI, et al. Cardiac specific PRMT1 ablation causes heart failure through CaMKII dysregulation. Nat Commun. 2018;9:5107.
27. Lai Y, Li X, Li T, Nyunoya T, Chen K, Kitsios GD, et al. Endotoxin stabilizes protein arginine methyltransferase 4 (PRMT4) protein triggering death of lung epithelia. Cell Death Dis. 2021;12:828.
28. Fang X, Cai Z, Wang H, Han D, Cheng Q, Zhang P, et al. Loss of cardiac ferritin H facilitates cardiomyopathy via Slc7a11-mediated ferroptosis. Circ Res. 2020;127:486–501.
29. Mancias JD, Wang X, Gygi SP, Harper JW, Kimmelman AC. Quantitative proteomics identifies NCOA4 as the cargo receptor mediating ferritinophagy. Nature. 2014;509:105–9.
30. Rojo de la Vega M, Chapman E, Zhang DD. NRF2 and the hallmarks of cancer. Cancer Cell. 2018;34:21–43.
31. Ichikawa Y, Ghanefar M, Bayeva M, Wu R, Khechaduri A, Naga Prasad SV, et al. Cardiotoxicity of doxorubicin is mediated through mitochondrial iron accumulation. J Clin Invest. 2014;124:617–30.
32. Zhang X, Hu C, Kong CY, Song P, Wu HM, Xu SC, et al. FNDC5 alleviates oxidative stress and cardiomyocyte apoptosis in doxorubicin-induced cardiotoxicity via activating AKT. Cell Death Differ. 2020;27:540–55.
33. Tadokoro T, Ikeda M, Ide T, Deguchi H, Ikeda S, Okabe K, et al. Mitochondria-dependent ferroptosis plays a pivotal role in doxorubicin cardiotoxicity. JCI Insight. 2020;5:e132747.
34. Harrison SA, Goodman Z, Jabbar A, Vemulapalli R, Younes ZH, Freilich B, et al. A randomized, placebo-controlled trial of emricasan in patients with NASH and F1-F3 fibrosis. J Hepatol. 2020;72:816–27.
35. Xu W, Chen H, Du K, Asahara H, Tini M, Emerson BM, et al. A transcriptional switch mediated by cofactor methylation. Science. 2001;294:2507–11.
36. Dai C, Chen X, Li J, Comish P, Kang R, Tang D. Transcription factors in ferroptotic cell death. Cancer Gene Ther. 2020;27:645–56.
37. Sun X, Ou Z, Chen R, Niu X, Chen D, Kang R, et al. Activation of the p62-Keap1-NRF2 pathway protects against ferroptosis in hepatocellular carcinoma cells. Hepatology. 2016;63:173–84.
38. La Rosa P, Petrillo S, Turchi R, Berardinelli F, Schirinzi T, Vasco G, et al. The Nrf2 induction prevents ferroptosis in Friedreich's Ataxia. Redox Biol. 2021;38:101791.
39. Sun Z, Chin YE, Zhang DD. Acetylation of Nrf2 by p300/CBP augments promoter-specific DNA binding of Nrf2 during the antioxidant response. Mol Cell Biol. 2009;29:2658–72.
40. Liu X, Li H, Liu L, Lu Y, Gao Y, Geng P, et al. Methylation of arginine by PRMT1 regulates Nrf2 transcriptional activity during the antioxidative response. Biochim Biophys Acta. 2016;1863:2093–103.
41. Yarmohammadi F, Rezaee R, Karimi G. Natural compounds against doxorubicin-induced cardiotoxicity: A review on the involvement of Nrf2/ARE signaling pathway. Phytother Res. 2021;35:1163–75.
42. Nordgren KK, Wallace KB. Keap1 redox-dependent regulation of doxorubicin-induced oxidative stress response in cardiac myoblasts. Toxicol Appl Pharm. 2014;274:107–16.

AUTHOR CONTRIBUTIONS

JH designed the study; YW, SY, LY, and PW performed the experiments; XL, FD, and LH analyzed the data; YW wrote the manuscript; KH and JH revised the manuscript.

COMPETING INTERESTS

The authors declare no competing interests.

ETHICS APPROVAL

No experiments involving human subjects were performed in this study. All animal experiments in this article were approved by the Animal Research Institute of Sun Yat-Sen University, China.

ADDITIONAL INFORMATION

Supplementary information The online version contains supplementary material available at https://doi.org/10.1038/s41418-022-00990-5.

Correspondence and requests for materials should be addressed to Kai Huang or Jiangui He.